



An electron-rich metal-organic framework for highly efficient photocatalytic reduction of Cr(VI)

Guiqin Niu , Chen Si , Jiachen Jiao , Qiuxia Han ^{*} , Mengfei Guo , Mingxue Li ^{**}

Henan Key Laboratory of Polyoxometalate Chemistry, Institute of Molecular and Crystal Engineering, School of Chemistry and Chemical Engineering, Henan University, Kaifeng, Henan, 475004, China



ARTICLE INFO

Article history:

Received 6 December 2019

Received in revised form

24 February 2020

Accepted 7 March 2020

Available online 9 March 2020

Keywords:

Metal-organic framework

Photocatalysis

Cr(VI) reduction

Electron-rich

ABSTRACT

A metal-organic framework, Cd-TIPA, was synthesized using cadmium ion and a stretched triangular rigid N-containing ligand tris-(4-imidazolylphenyl)amine (TIPA) as a strong electron donor. Cd-TIPA features an unusual 3D structure of two sets of layers linked in an interpenetration arrangement, resulting in framework with 26.1% porosity. Cd-TIPA possesses a long luminescence lifetime of 5.76 μs and Mott-Schottky measurements indicate Cd-TIPA is a representative n-type semiconductor. Cd-TIPA features a potential of the conduction band (LUMO) level (-1.30 V vs. NHE), which is more negative than that of Cr₂O₇²⁻/Cr³⁺, thus providing the theoretical possibility of reduction. The valence band (HOMO) level is estimated as 1.37 V based on a Tauc plot, indicating a higher oxidation ability for H₂O. The observable quenching effect of Cr₂O₇²⁻ anions on the emission of a suspension of Cd-TIPA indicates the efficient electron transfer. As expected, Cd-TIPA functioned as an efficient catalyst for heterogeneous photocatalytic reduction of Cr₂O₇²⁻ with high catalytic efficiency (93%) in 12 min.

© 2020 Elsevier B.V. All rights reserved.

1. Introduction

The rapid development of chemical industries has resulted in serious water pollution, especially due to the massive use of heavy metals in electroplating, paint processes, mining, and the manufacturing of electronic products [1–3]. Heavy metals are toxic in nature and severely threaten the environment and human health. There is a significant interest in the design and synthesis of functional materials for the remediation of heavy metals. Luo et al. applied organo-functionalized silica nanoparticles for the adsorption of heavy metal ions in a facile silylation reaction [4]. This group also developed defective ZrO₂ using a facile-controlled crystallization strategy, and the resulting material exhibited effective adsorption of arsenic [5]. Luo et al. also applied polymeric adsorbent PAR(poly-allylrhodanine) for the recovery of Ag⁺ ions by the adsorption sites of C=S and C–S groups on PAR [6]. The hexavalent chromium anion Cr(VI) is one of the most toxic heavy metal contaminants [7,8]. Therefore, rapid and efficient detection and reduction of trace Cr(VI) anions in water are particularly urgent.

Many methods have been applied for the removal of Cr(VI) from water, including chemical precipitation, biosorption, ion exchange, electrolysis, adsorption and electrochemical reduction [9–12]. However, these traditional methods are limited by disadvantages such as high-cost, secondary pollution, complex synthesis processes and inefficiency at lower concentrations [13]. Chromium exists in Cr(VI) and Cr(III) oxidation states in the natural environment, and Cr(III) is less toxic and an essential trace element for humans [14,15]. Therefore, a reasonable approach to reducing the amounts of Cr(VI) is not to absorb it but to degrade/reduce it to the safer Cr(III) [16]. Significant efforts have been made to develop photocatalysis strategies for the reduction of Cr(VI) ions to Cr(III) ions [17]. Periakaruppan's group reported PANI/MnO₂/TiO₂ as an effective catalyst for the reduction of Cr(VI) [18]. Han's group explored the photocatalytic activity of Ti³⁺ self-doped TiO₂ nanoparticles to treat effluent containing Cr under visible light, where the ethylene glycol on the surface of TiO₂/Ti(III) served as a sacrificial agent [19]. Liang's group designed a Ce³⁺ doped CeO₂/Bi₂MoO₆ (C-BMO) heterojunction, which removed up to 97% dichromate Cr(VI) due to interfacial movement of photogenerated e⁻-h⁺ pairs between the generated Ce³⁺/Ce⁴⁺ redox couple [20].

Metal-organic frameworks (MOFs) with diverse structures, high porosity, and adjustable functionality have been applied for gas storage, magnetism, optical material, and chemical sensing. These

* Corresponding author.

** Corresponding author.

E-mail addresses: qiuxia_han@163.com (Q. Han), [\(M. Li\).](mailto:limingxue@henu.edu.cn)

materials also widely used in catalysis, because they provided a good platform to study reaction mechanism at the molecular level during catalytic application [21–23]. Photocatalytic MOFs have been developed and applied in water splitting, CO₂ reduction, and the degradation of organic and inorganic pollutant [24–27].

To prepare a photocatalytic MOF specific for Cr(VI) reduction, an organic link with specific photochemical and photophysical properties is required. TIPA has a large volume and various coordination modes, and as a strong electron donor, which can stabilize the charge transferred state, and also displays good hole-transporting ability to modify the electrical conductivity of materials [28,29]. Next, the metal ions should be carefully selected for the photocatalytic MOF. Cd(II) ion has high ligand field stabilization energy, excellent fluorescence performance, and good conductive catalytic properties, enabling it use in constructing stable MOFs. Recently, Li et al. explored a Cd-TBAPy MOF as a photocatalyst for both water reduction and oxidation under visible light [30]. Cheng et al. synthesized (MOFx)/P–TiO₂ hybrid composites using phosphonate-based MOF [Cd(H₂L)]_n and phosphated mesoporous TiO₂ beads and showed that Cd-MOF could effectively improve the degradation of pollutants [31]. Ali Morsali et al. designed a tunable conductive MOF with additional well-dispersed Cd(II) into a valid sorbent MOF (TMU-60) with enhanced electron transport available [32]. Based on these findings, combining TIPA moieties and d¹⁰ metal ions Cd(II) in a single framework would permit unusual metal-ligand charge transfer and fluorescence performance, compared to traditional metal oxide semiconductors. Recent work using TIPA-based MOFs has mainly focused on the highly selective adsorptive separation of small molecule hydrocarbons, luminescent sensors, photocatalytic degradation of dyes, and the detection and extraction of Cr(VI) species, but few studies have examined the photocatalysis of Cr(VI) ions [33,34].

In this work, a photocatalyst Cd(TIPA)(NO₃)₂·H₂O (Cd–TIPA) was assembled by combining the organic ligand TIPA with Cd(NO₃)₂ under hydrothermal conditions. Although Cd–TIPA was reported by Zheng's group, only the structure was described in detail [35]. In this work, we synthesized the material and studied its use for catalysis. Because Cd–TIPA is a typical n-type semiconductor with a more negative LUMO level (−1.30 V vs. NHE) than that of Cr₂O₇^{2−}/Cr³⁺, we envisioned that incorporation of TIPA as a reduction catalyst into a MOF would allow effective photocatalytic Cr(VI) reduction.

2. Experimental

2.1. Synthesis and methods

The Cd-TIPA was synthesized as described [35]. Crystals were obtained with a yield of 70% (based on TIPA ligand). Elemental analyses (EA) and Inductively Coupled Plasma (ICP) calcd (%) for C₂₇H₂₁CdN₉O₇: C 46.60, H 3.04, N 18.11, Cd 16.15; Found: C 46.65, H 3.10, N 18.01, Cd 16.10.

All solvents and chemicals were commercially purchased and directly used. EA of C, H, and N were performed on a Vario EL III elemental analyzer. ICP analysis was performed on a Jarrel-Ash J-A1100 spectrometer. Infrared spectra (IR) were recorded from a solid sample pelletized with KBr on JASCO FT/IR-430 in the range of 4000–400 cm^{−1}. Powder X-ray diffractograms (PXRD) were obtained on a Rigaku D/Max-2400 with Cu K α radiation ($\lambda = 1.5418 \text{ \AA}$) in the angular range $2\theta = 5\text{--}50^\circ$ at 293 K. X-ray photoelectron spectroscopy (XPS) analyses were performed on an ESCALAB 250 XI (Thermo Fisher, USA) spectrometer with an Al Ka ($h\nu = 1486.6 \text{ eV}$) achromatic X-ray source. Vacuum inside the analysis chamber was maintained at $1 \times 10^{-9} \text{ Pa}$ during analysis. N₂ absorption-desorption isotherms for determining the

Brunner–Emmett–Teller (BET) surface area and Barrett–Joyner–Halenda (BJH) pore width distribution were obtained with an ASAP 2460 Micromeritics instrument, using N₂ as the adsorbent at 77 K. UV–vis diffuse reflectance spectra (DRS) were collected at room temperature on a finely ground sample with a HITACHI U-4100 UV–Vis–NIR spectrometer equipped with a 60 mm diameter integrating sphere. Photoluminescence (PL) properties were performed on EDINBURGH FLS 980 fluorescence spectrophotometer equipped with a 450 W xenon lamp. UV–Vis absorption spectrum was recorded with a TU-1900 spectrometer at room temperature. Mott–Schottky measurements carried on a CHI 760E electrochemical workstation (Shanghai Chenhua Instrument Co., China) in a three-electrode electrochemical cell using a 0.1 M Na₂SO₄ as the electrolyte. The photocatalytic reactions were performed on WATTCAS Parallel Light Reactor (WP-TEC-1020HSL) with 10W COB LED.

2.2. Photocatalytic activity measurement

K₂Cr₂O₇ and KMnO₄ was selected as the sources of Cr(VI) and Mn(VII), respectively, and photocatalytic reduction was carried out under white light irradiation. The typical process was performed as follows: 5 mg of catalyst Cd–TIPA was dispersed in 5 mL of a Cr(VI) or Mn(VII) aqueous solution, at the initial concentration of 0.5 and 1.0 mmol/L, respectively. Then, a 10 W white LED lamp was used to irradiate the mixed solution. The supernatant was obtained through centrifugation after different amounts of irradiation time. The catalysts and supernatant were recovered in a quartz tube for the photocatalytic experiment. The photocatalytic process of the compound was monitored by determination of the UV–vis absorption spectrum.

3. Results and discussion

3.1. Structural description

Single-crystal X-ray diffraction structural analysis showed that Cd–TIPA crystallizes in the space group C₂. There was one crystallographically independent cadmium ion, one TIPA ligand, two NO₃[−], and one free H₂O in the asymmetric unit of Cd–TIPA. The cadmium ion exhibits a distorted pentagonal bipyramidal geometry by coordinating with three N atoms from individual TIPA ligands [Cd(1)–N: 2.294(11)–2.311(10) Å], and four oxygen atoms from two NO₃[−] anions [Cd(1)–N: 2.420(6)–2.656(9) Å] (Fig. 1a). The central N(3) atom exhibits sp² hybridization rather than sp³ hybridization, based on C–N(3)–C angles of 118.3(9), 119.5(9) and 122.3(10)°. The lone pair electrons of N atom located in the p orbital have higher energy, with movement throughout the big π bond, thus making Cd–TIPA conductive [36]. Each TIPA bridges three Cd(II) centers to construct a 2D honeycomb network (Fig. 1b). The 2D layers are packed by parallel arrangement furnishing a 1D hexagonal nano-channel of 20.88 Å × 16.77 Å viewed along the c direction (Fig. 1c). More interesting, two sets of 2D layers further connect in tilted interpenetration with a 60.58° dihedral angle to form a 3D catenation framework with a porosity of 26.1% (954.7 Å³) (Fig. 1d–f) [37]. The interpenetration structure apparently strengthens the stability of the framework. The N₂ adsorption–desorption isotherms indicate the BET (Brunauer–Emmett–Teller) surface area and pore volume of Cd–TIPA were 8.158 m²/g and 0.017 cm³/g, respectively (Fig. 2a). The pore diameter distribution of Cd–TIPA is 2.769 nm, corresponding to the mesopores, which can increase the adsorption and transfer of heavy metal ions Cr(VI) [7,10].

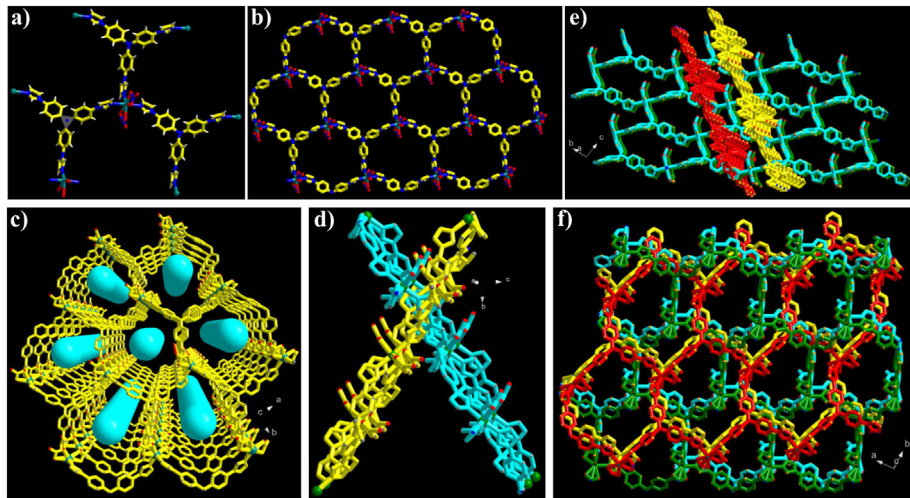


Fig. 1. (a) The coordinate environment of Cd(II) ion. (b) The single 2D layer of Cd–TIPA. (c) The packing of Cd–TIPA with 1D hexagonal nanotube-like channels by parallel-parallel arrangement. (d) Two-fold interpenetration through two sets of 2D layers of the Cd–TIPA with a dihedral angle of 60.58°. (e, f) The 3D structure of interpenetrating networks along the *a* or the *c* axis. (hydrogen atoms and free water are omitted for clarity).

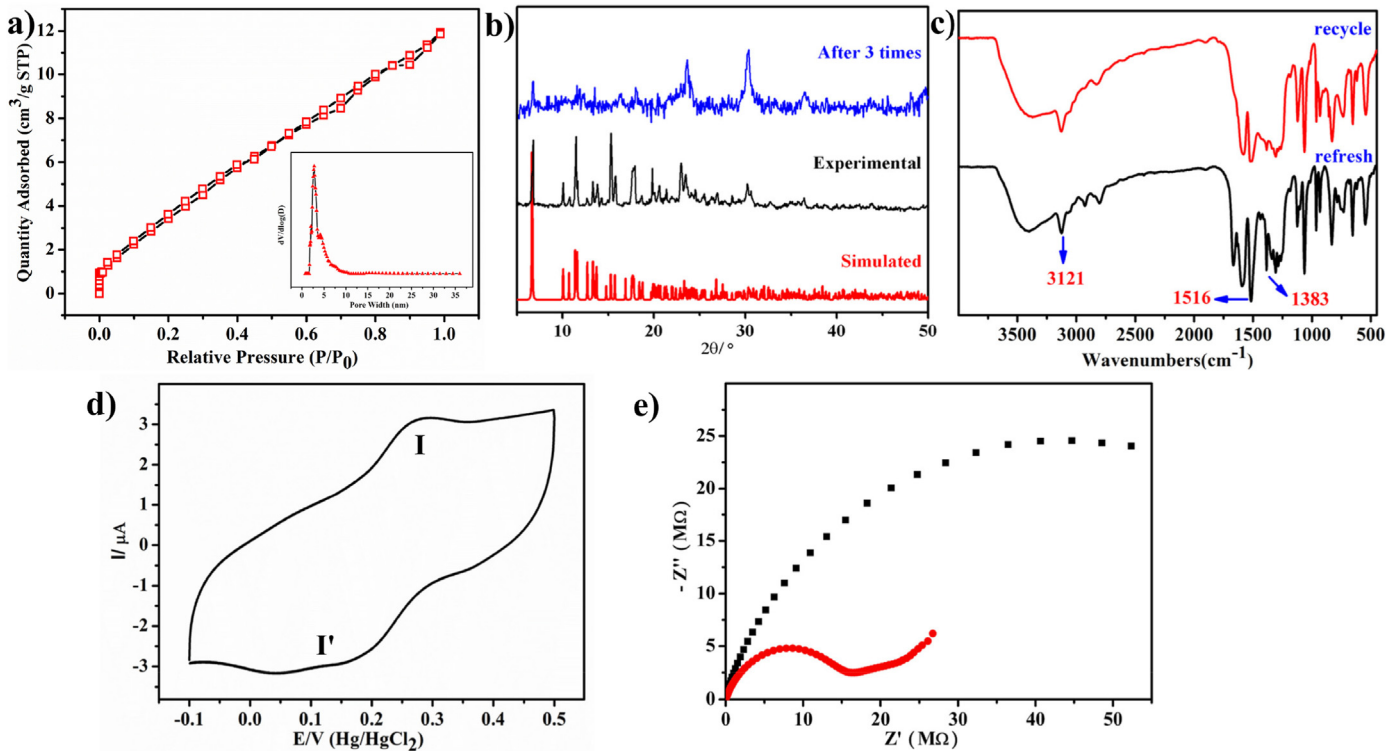


Fig. 2. (a) N_2 sorption isotherm of Cd–TIPA. Inset: the pore-size distribution of Cd–TIPA (right bottom) (b) PXRD of Cd–TIPA. (Simulated, Experimental and Recovery catalyst after three runs) (c) IR spectra of the fresh and recovered Cd–TIPA (d) CV of Cd–TIPA in the 1.0 M Na_2SO_4 – H_2SO_4 aqueous solution (scan rate: 100 mV/s). (e) Nyquist diagram from EIS tests of the fresh (black closed squares) and reduced sample (red open circles, right/top axes), respectively. (For interpretation of the references to color in this figure legend, the reader is referred to the Web version of this article.)

3.2. IR spectra, PXRD diffractograms and electrochemical properties

As can be seen from PXRD pattern of Cd–TIPA, the experimental pattern is highly consistent with its calculated pattern based on the single-crystal solution, indicating the pure phase of its bulk samples (Fig. 2b). The IR spectral data were collected for Cd–TIPA, as shown in Fig. 2c. The band at 3423 cm^{-1} is assigned to the $\nu(O-H)$ of the free water molecules. The characteristic peaks in the ranges

of 1055 – 1383 and 2938 – 3121 cm^{-1} are mainly ascribed to the TIPA ligand and the peak at ca. 1516 cm^{-1} is attributed to stretching vibrations of imidazole groups [38,39]. The band at 1383 cm^{-1} is assigned to the characteristic absorption of NO_3^- [40].

The cyclic voltammogram (CV) of a carbon paste electrode modified with Cd–TIPA is shown in Fig. 2d. A pair of quasi-reversible redox peaks located at $E_{ox} = 0.277\text{ V}$ and $E_{red} = 0.170\text{ V}$ are corresponding to the redox of TIPA. As literature

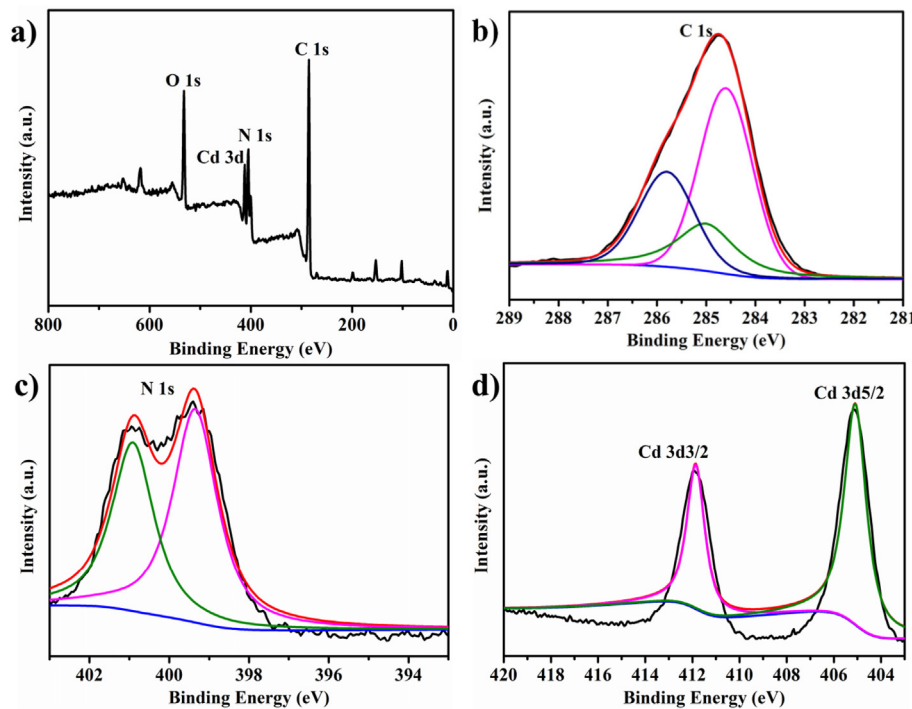


Fig. 3. The XPS spectra of Cd–TIPA: (a) survey spectrum, (b) high resolution C 1s, (c) high resolution N 1s and (d) high resolution Cd 3d.

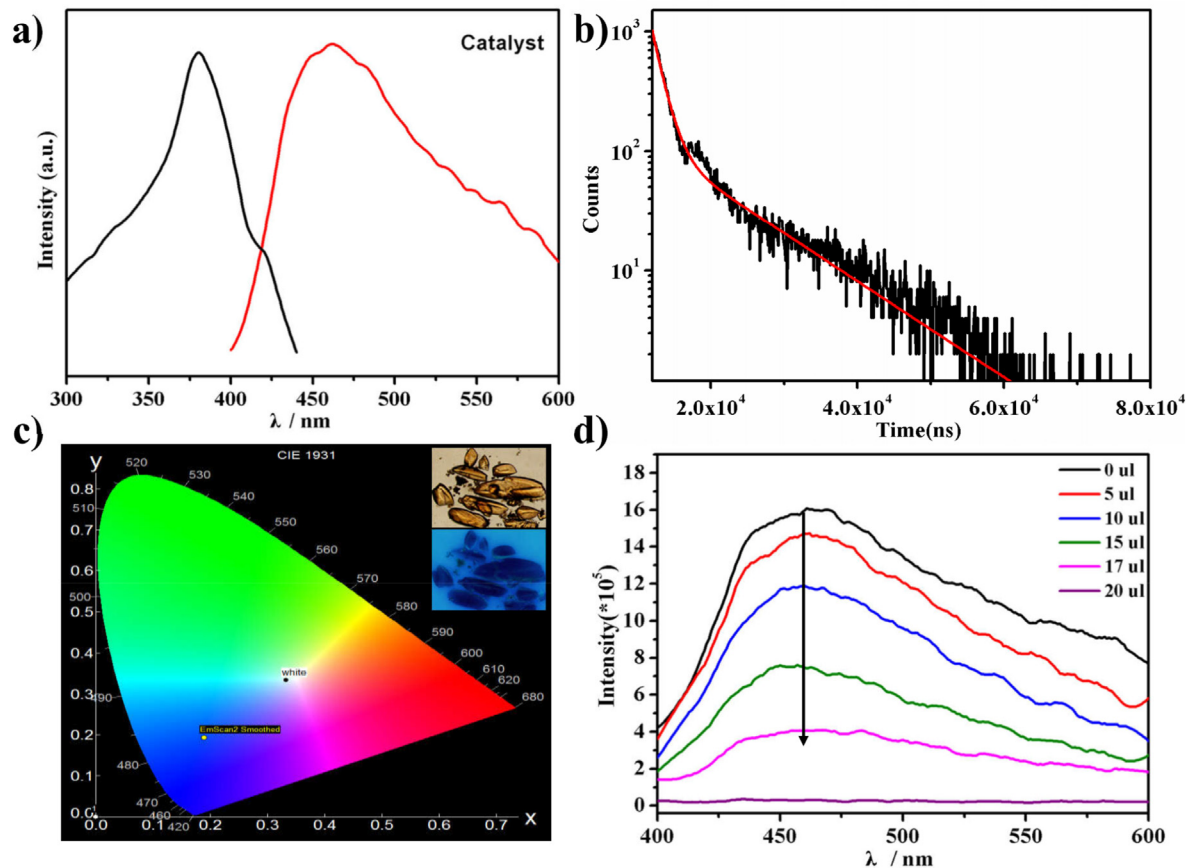


Fig. 4. (a) Excited (black) and emission (red) spectra of Cd–TIPA at room temperature. (b) The luminescence decay curve of Cd–TIPA. (c) The CIE chromaticity diagram of the emissions of Cd–TIPA. Inset: Bright field images (top), confocal laser scanning micrographs (bottom) at $\lambda_{ex} = 325$ nm of Cd–TIPA. (d) Emission spectra of Cd–TIPA with different additions of Cr₂O₇²⁻ ions. (For interpretation of the references to color in this figure legend, the reader is referred to the Web version of this article.)

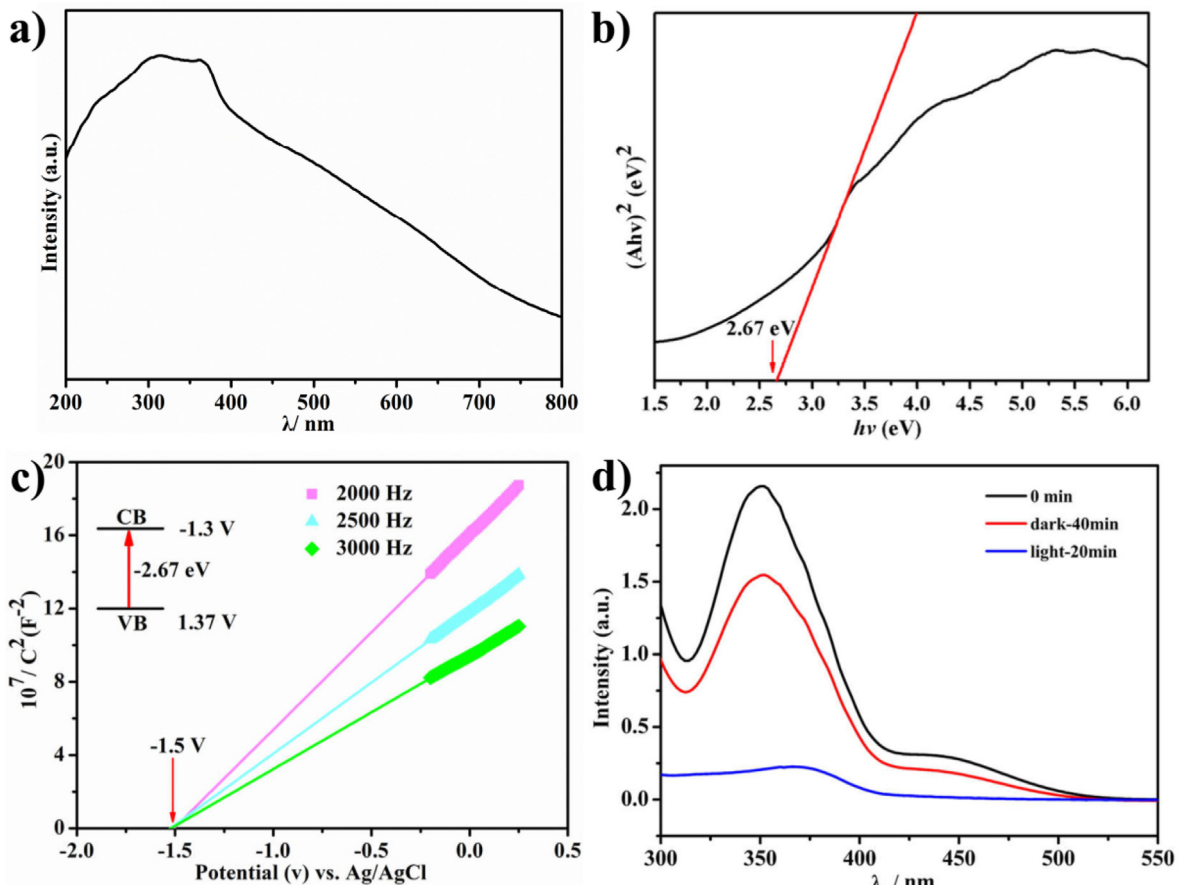


Fig. 5. (a) Solid UV–vis absorption data of Cd–TIPA. (b) The Tauc plots of Cd–TIPA. (c) Mott–Schottky plots for Cd–TIPA in 0.1 M Na_2SO_4 aqueous solution. Insets are the energy diagrams of the VB and CB levels of Cd–TIPA. (d) The adsorption equilibrium plot of Cd–TIPA in 0.5 mmol/L $\text{K}_2\text{Cr}_2\text{O}_7$ for 40 min in dark.

reported, the introduction of triphenylamine groups into the conjugated compounds can enhance the hole injection characteristics of the materials [41]. When applied voltage, the electron-rich triphenylamine groups in the compounds will be oxidized, thus making the N atoms with higher electron density lost electrons. The charge transfer properties at the electrode/solution interface were examined by electrochemical impedance spectroscopy (EIS). The EIS Nyquist plots of Cd–TIPA before and after photo-irradiation assessed the proton conductivity of the powdered crystalline sample at 298 K and relative humidity. As shown in Fig. 2e, the semicircle portion corresponds to the charge transfer process. The powdered crystalline sample after photo-irradiation shows a higher conductivity, $1.59 \times 10^{-8} \text{ S} \cdot \text{cm}^{-1}$, compared to fresh samples (3.3×10^{-9}), suggesting that the Cd–TIPA can facilitate charge transfer. The addition of excess electrons to porous materials is an important strategy to switch the electronic properties such as conductivity [2].

3.3. XPS study

The electronic environment and structure of Cd–TIPA were also investigated by XPS. The XPS spectra indicate the presence of C, N, O and Cd in Cd–TIPA (Fig. 3a). The C 1s spectra can be divided into three peaks at 284.6, 285.0, and 285.8 eV ascribed to the C atoms in the TIPA ligand of (C–H)/(C–C), (C=C) and (C–N), respectively (Fig. 3b). The N 1s spectra at ca. 399.30 eV and ca. 400.90 eV can be assigned to the pyridinic N (C–N–C) and amino N (N–(C)₃), respectively (Fig. 3c). Pyridinic N atom could reduce the energy

barrier and accelerate electron transfer, thus enhancing catalytic performance in oxidation-reduction reactions [42]. The peaks at 405.5 and 412.3 eV are assigned to the binding energies of Cd 3d_{5/2} and Cd 3d_{3/2} (Fig. 3d) respectively, displaying Cd in +2 oxidation state [43]. With full 4d orbitals and empty 5s orbitals of Cd, the contribution on orbitals is negligible compared with the N 2p and C 2p orbitals originating from organic linkers. We conclude that TIPA plays a vital role in band composition and position, so using TIPA allows Cd–TIPA to achieve both Cr(VI) reduction and water oxidation [30].

3.4. Luminescent properties

The powder photoluminescent properties of Cd–TIPA were investigated at room temperature. Cd–TIPA shows a broad band with a peak at 465 nm upon excitation at 381 nm (Fig. 4a). Because of the coordination of ligand with the metal center, the emission exhibits a red-shift compared with TIPA. The coordination enhances the rigidity of the ligand and weakens the loss of energy by radiationless decay [44]. Due to the d¹⁰ configuration of Cd²⁺, the emission band is neither metal-to-ligand charge transfer (MLCT) nor ligand-to-metal transfer (LMCT) in nature [45]. Thus, the emission can be assigned as ligand-centred $\pi^* \rightarrow \pi$ transitions of the TIPA ligands [46]. According to the above observations, this stable polymer material may be applied for potential photoactive materials. The fluorescence lifetime of Cd–TIPA was also studied. The lifetime curve of Cd–TIPA was be fitted with a double exponential function (Fig. 4b) [47].

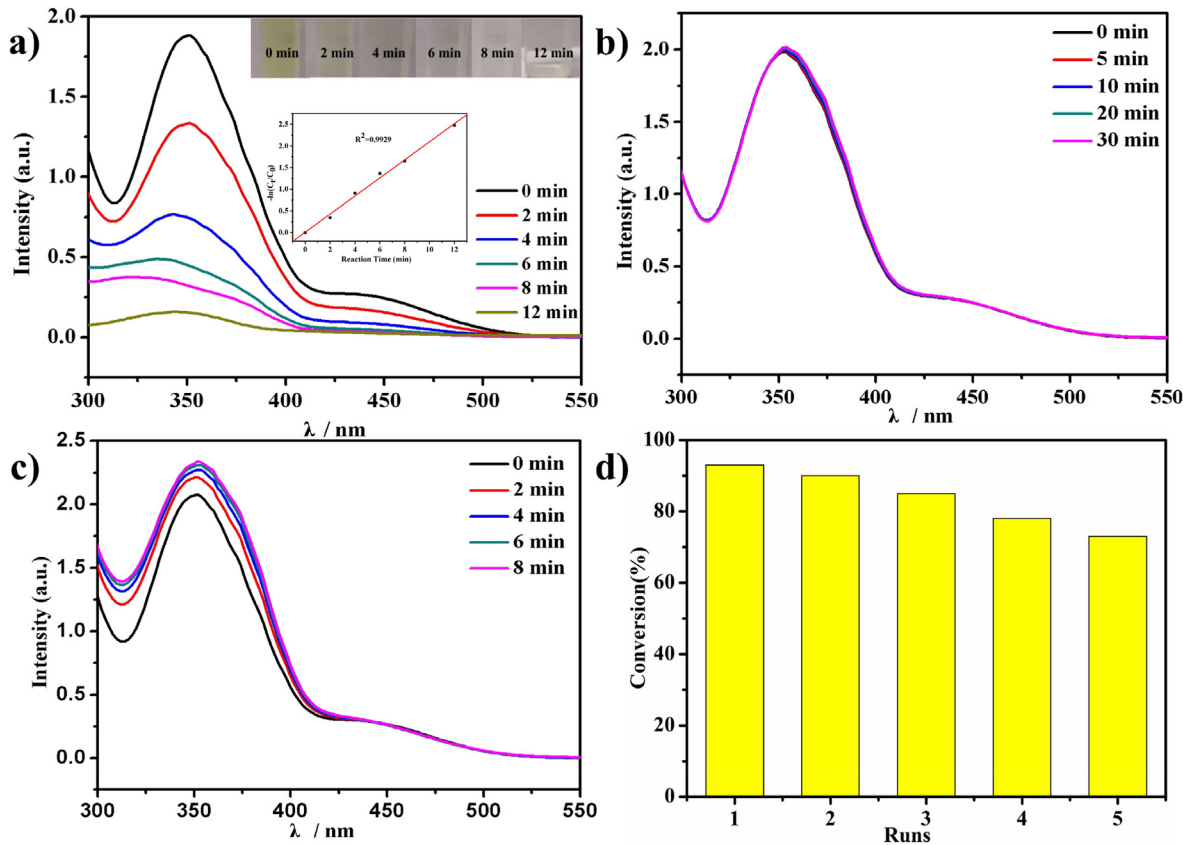


Fig. 6. (a) UV–visible absorbance spectra of Cr(VI) with Cd–TIPA photoreduction at intervals. Inset: Kinetic plot of reduction of Cr(VI). C_t is the observed concentration, and C_0 is the initial concentration. (b) Control experiment without catalyst. (c) Photocatalytic reduction of Cr(VI) with TIPA as catalyst. (d) Recyclability tests of Cd–TIPA catalyst for photocatalytic reduction of Cr(VI).

Table 1

Comparison of Cd–TIPA with various catalysts for the photocatalytic reduction of Cr(VI).

Catalyst	T, °C	Dosage of catalyst(mg)	Concentration of Cr(VI) (mg L ⁻¹)	Volume of Cr(VI) solution solvent (mL)	light source	t, min	k_{obsd} , min ⁻¹	ref	
Cd–TIPA	r.t.	5 mg	147	5	H_2O	10W white LED lamp	8	0.22	this work
[Cu ₄ (bpy) ₄][β-As ₈ V ₁₄ O ₄₂ (H ₂ O)]	50	20 mg	3.57×10^{-4}	500	H_2O and Formic acid none	30	0.043	15	
[Ag ₄ (H ₂ O)(L) ₃ SiW ₁₂ O ₄₀] r.t.	50 mg	80	100	H_2O and isopropanol	visible light	160	0.0126	17	
H ₂ TCPP \subset (I ⁻)Meim-UiO-66	r.t.	10	100	40	H_2O and HCl or NaOH	300W Xe lamp	30	0.1541	51
CeO ₂ /Bi ₂ MoO ₆ (C-BMO)	r.t.	50	10	50	H_2O	5W white LED	90	0.04113	20
PANI/MnO ₂ /TiO ₂	45	1.0	588	10	H_2O and Formic acid	none	5	0.1597	18

Ref listed as number only is corresponding to the references in main body.

r.t. Represents room temperature.

The luminescence lifetimes τ_1 and τ_2 were 1.39 μs (53.5%) and 10.78 μs (46.5%), respectively, and the agreement factor (χ^2) was 1.058. The luminescence lifetime was determined by application the following equations: $\tau_i = \frac{\sum \alpha_i \tau_i^2}{\sum \alpha_i \tau_i}$. The luminescence of Cd–TIPA has an average lifetime of around 5.76 μs at room temperature. The CIE chromaticity coordinate for Cd–TIPA was calculated by its corresponding visible PL spectra and was indexed to (0.18932, 0.19354), which is located in the blue region (Fig. 4c) [48]. The calculated color purity of Cd–TIPA is 61.8%, and the correlated color temperature is 8081 K. The emission intensities of Cd–TIPA decreased dramatically with increasing Cr₂O₇²⁻ amounts from 0 to

20 μL, which indicates efficient electron transfer (Fig. 4d).

3.5. UV–vis, Band gap energy and Mott-Schottky plot

The optical absorption properties of the Cd–TIPA powder samples were investigated by UV–vis (Fig. 5a). The UV–vis spectrum displays a major absorption broad band near 250–500 nm. The band gap of Cd–TIPA was estimated at 2.67 eV using the Kubelka–Munk function as described (Fig. 5b) [49]. The variation of the energy band for Cd–TIPA was validated by investigating its flat band potential. The positive slopes of the linear parts are consistent

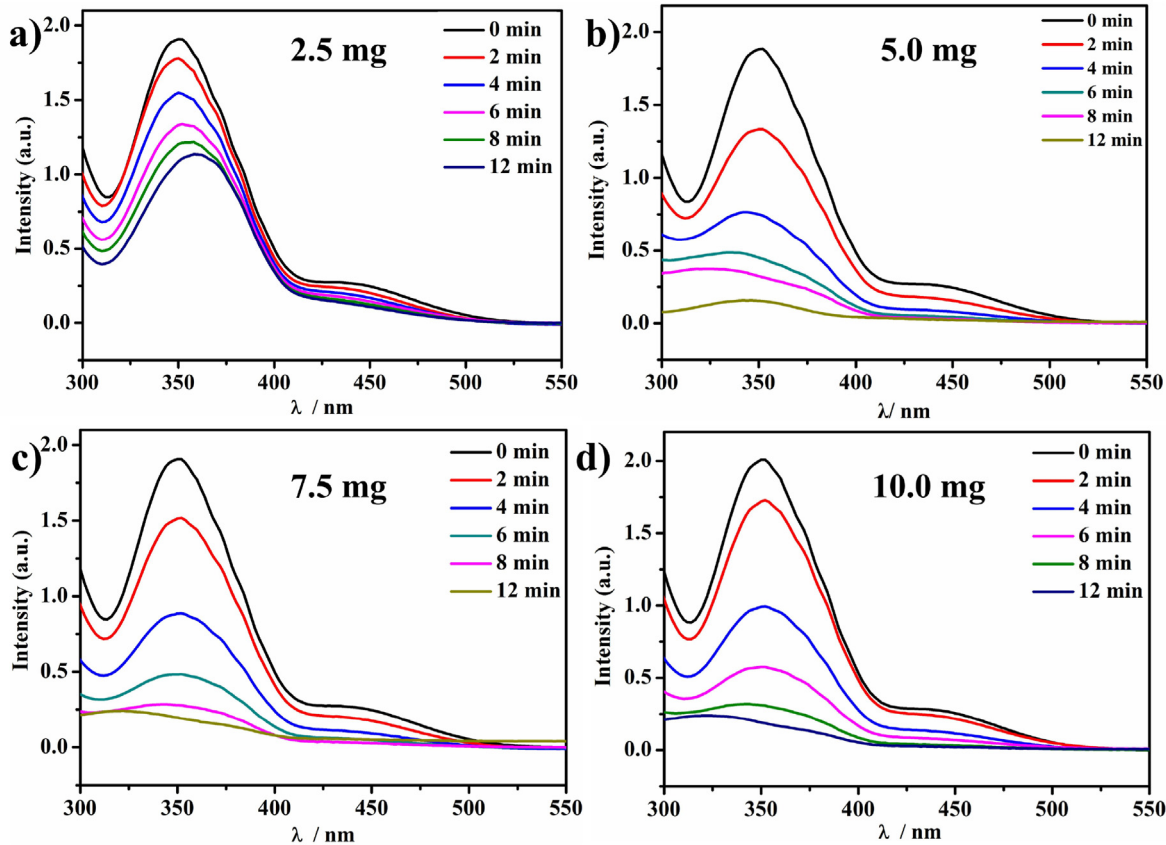


Fig. 7. (a-d) Photocatalytic reduction of Cr(VI) with variable Cd-TIPA content of 2.5 mg, 5.0 mg, 7.5 mg, 10 mg.

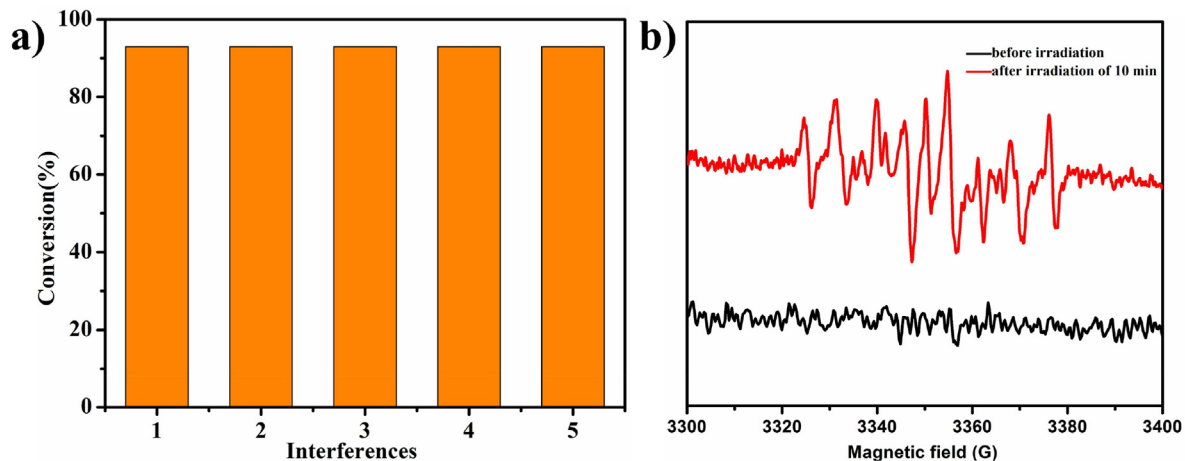


Fig. 8. (a) Effect of foreign ions on catalytic conversion: KCl (1), Na_2SO_4 (2), KNO_3 (3), glucose (4), and citric acid (5). (b) ESR spectra of O_2^{\bullet} radical trapped by 5-dimethyl-pyrroline-N-oxide (DMPO).

with n-type semiconductor features. The flat band potential of Cd-TIPA was estimated as -1.50 V (vs Ag/AgCl) (Fig. 5c). Calculated by the equation, $E_{\text{CB}} = E(\text{vs Ag/AgCl}) + 0.2 \text{ V}$, the conduct band potential (E_{CB}) value of Cd-TIPA was -1.30 V (vs NHE) for Cd-TIPA. Based on the formula $E_{\text{VB}} = E_{\text{CB}} + E_g$ [50] the E_{VB} value of Cd-TIPA can be estimated as 1.37 eV according to the results of UV-vis absorption spectra and electrochemical tests. Obviously, the E_{CB} potential values of the prepared compound is more negative than the standard redox potential of Cr(VI)/Cr(III) [20] (0.51 eV vs. NHE),

indicating that the photogenerated electrons can easily transfer to $\text{Cr}_2\text{O}_7^{2-}$ for photoreduction.

3.6. Catalytic activity for Cr(VI) reduction

The activity of Cd-TIPA was investigated for catalytic reduction of Cr(VI) by visible light irradiation. Initially, the adsorption experiment was preformed with $0.5 \text{ mmol/L K}_2\text{Cr}_2\text{O}_7$ in the dark for 40 min. Near the adsorption equilibrium, the Cr(VI) adsorption

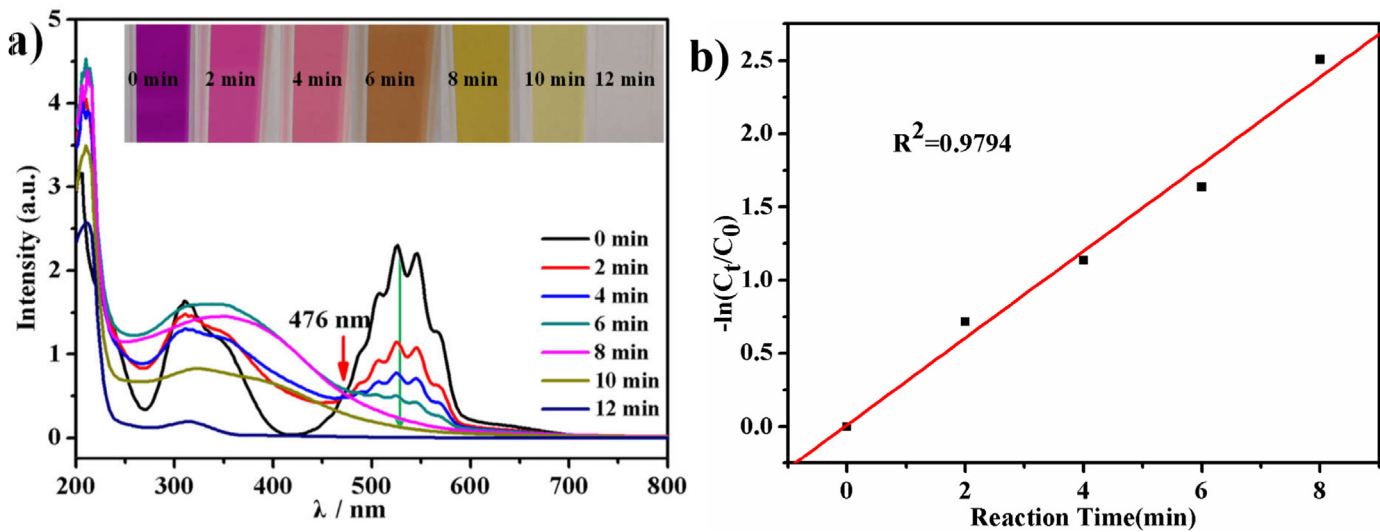


Fig. 9. (a) UV-visible absorbance spectra of Mn(VII) with Cd-TIPA photoreduction under visible light. (b) Kinetic plot of reduction of Mn(VII), C_t is the observed concentration, and C_0 is the initial concentration.

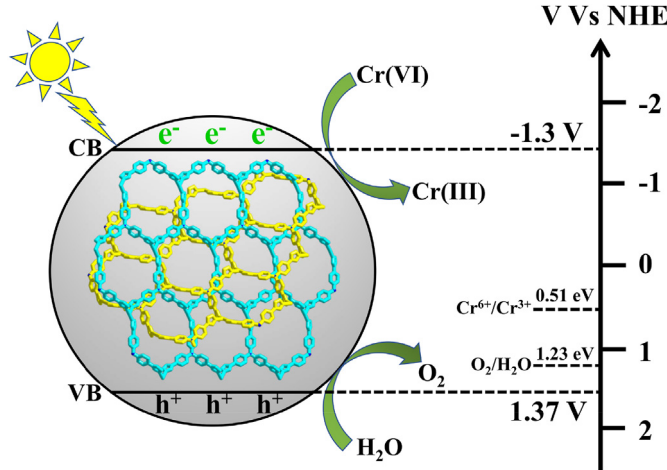


Fig. 10. Proposed photocatalytic process for Cd-TIPA under visible light irradiation.

percentage was about 28.2%. The solution was then irradiated with a 10 W white LED lamp for 20 min, indicating the almost complete reduction of Cr(VI) to Cr(III) as the final product (Fig. 5d). Encouragingly, when not reaching adsorption equilibrium, Cr(VI) was reduced 93% in a shorter time (12 min) by direct irradiation without any cocatalyst and sacrificial agent (Fig. 6a). The plot of $-\ln(C_t/C_0)$ against time indicates that the reduction of the Cr(VI) proceeds with apparent pseudo-first-order rate kinetics with a constant k_{obsd} of $2.1 \times 10^{-1} \text{ min}^{-1}$. Cd-TIPA performance for the photo-reduction of Cr(VI) was compared with that of previously reported catalysts and showed outstanding performance of Cd-TIPA in reaction time and reaction rate (Table 1). For example, the POM-based material [$\text{Ag}_4(\text{H}_2\text{O})_6\text{L}_3(\text{SiW}_{12}\text{O}_{40})$] required 160 min reaction time with an apparent rate constant of only $1.26 \times 10^{-2} \text{ min}^{-1}$ [17].

Photocatalytic reduction of Cr(VI) was explored with variable Cd-TIPA content of 2.5 mg, 5.0 mg, 7.5 mg, 10 mg, respectively (Fig. 7). The photo-reduction rate was low at a lower concentration of catalyst, but a high concentration of catalyst resulted in a better photo-reduction rate. The photo-reduction (%) increased to a certain value and thereafter remained nearly constant for catalyst doses up to 5 mg. These results strongly demonstrate increased

photon absorption with increased content of the catalyst, with higher catalyst dose hindering photoelectron transfer. The optimal amount of catalyst for the reaction process was 5 mg of catalyst. The control experiments indicated that the reduction of Cr(VI) is inert in the absence of light or Cd-TIPA. When only TIPA was employed as a catalyst, the absorbance exhibited an atypical rising trend. The great performance of Cd-TIPA might reflect the transformation of electron donor TIPA into a rigid MOF, which can increase the probability of photo-induced electron transfer and can stabilize the charge-transferred state [51]. The sp^2 hybridization of the central nitrogen atom is also conducive to electron excitation from the ground state, thus improving the overall reduction rate [36]. The Cd-TIPA solids can be easily isolated from the reaction suspension by simple centrifugation. After five use cycles, the transformation rate showed a moderate decrease from 93% to 73% (Fig. 6d), which is likely indicating the possible leaching of Cd(II) or organic ligand.

We also explored the influences of foreign ions upon the catalytic reduction reaction because wastewater usually contains a mixture of organic and inorganic substances. The presence of 1 mM of interferents such as KCl, Na₂SO₄, KNO₃, glucose, and citric acid had no significant effect on the photocatalytic reduction Cr(VI) using Cd-TIPA (Fig. 8a). This is because the inorganic cations (K⁺ and Na⁺) with the stable and maximum oxidation states do not consume electrons or holes, [52] and the organic molecules of glucose and citric acid cannot interact with Cr(VI) [18].

Theoretically, Cd-TIPA possesses more negative potential of VB than the reduction potential of O₂ to O₂⁻ (ROS, E(O₂/O₂⁻) = -0.33 V vs. NHE), it should facilitate O₂⁻ generation. The ESR spectral analysis was performed using 5-dimethyl-pyrroline-N-oxide (DMPO) as the classical O₂⁻ probe and showed atypical signals of O₂⁻ (Fig. 8b). With addition of the O₂⁻ scavenger *p*-Benzoquinone (BQ), [25] an 87% conversion (decreased 6%) was observed for the same conditions, which verified that O₂⁻ plays a synergistic role in the photocatalytic reduction of Cr₂O₇²⁻ [53,54]. However, under N₂ atmosphere, a negligible effect on the reduction of Cr⁶⁺ was observed, so we concluded that the O₂⁻ arises from the water oxidation process. The generated O₂⁻ maybe oxidize TIPA and destroy the stability and reusable performance of Cd-TIPA. The PXRD and IR results for recovery catalyst after five runs were different from those for fresh samples although the main peaks remained (Fig. 2b and c).

The reduction of high valence manganese Mn(VII) was also investigated. Mn(VII) was completely reduced within 12 min with the Cd–TIPA catalyst. As shown in Fig. 9a, the absorption of Mn(VII) at 526 nm and 546 nm continuously decreased with reaction time, accompanied by a color change from purple to red, then followed by yellow-brown, and finally colorless transparent solution, indicating the Mn oxidation state changes from heptavalence to sexavalence, and finally bivalence. Interestingly, the reaction exhibited a clear isosbestic point at 476 nm, demonstrating the redox reaction proceeds smoothly without formation of multiple products [55]. The absorbance intensities at 526 nm were measured, allowing calculation of the apparent rate constant value of 0.29 min^{-1} base on the slope of $-\ln(C_t/C_0)$ against time. This value indicates the catalytic effectiveness, which only depends on the reaction conditions employing (Fig. 9b). Clearly, the compound exhibits remarkable photocatalytic activity for Mn(VII) reduction.

3.7. Mechanism

Based on the results, a possible photocatalytic mechanism of Cd–TIPA is presented (Fig. 10). The π -orbital of TIPA serves as HOMO corresponding to the VB, and the π^* -orbital serves as the LUMO corresponding to the CB. Upon irradiated with light radiation, electrons get excited from VB to CB due to $\pi-\pi^*$ transition. The excited electrons on the TIPA units can easily transfer to the $\text{Cr}_2\text{O}_7^{2-}$ anions [56]. The obvious quenching phenomenon of the catalyst with the increase of $\text{Cr}_2\text{O}_7^{2-}$ concentration further verified the obvious electron transfer between Cd–TIPA and $\text{Cr}_2\text{O}_7^{2-}$ anions [11]. The more negative potential of VB of Cd–TIPA compared to that of $\text{E}(\text{O}_2/\text{O}_2^-)$ makes O_2^- generation theoretically possible [54,57]. The above control experiments verified O_2^- plays a synergistic role in the photocatalytic reduction of $\text{Cr}_2\text{O}_7^{2-}$, and the O_2^- is mainly derived from the water oxidation process. The higher E_{VB} value of Cd–TIPA compared to that of $\text{E}(\text{O}_2/\text{H}_2\text{O})$ provides theoretical support for water oxidation, thereby providing electrons to promote catalytic cycle completion.

4. Conclusions

In summary, an electron-rich MOF for highly efficient photoreduction of Cr(VI) was synthesized by incorporation of the excellent functional organic ligand TIPA under mild conditions. The prepared Cd–TIPA photocatalyst exhibited photocatalytic performance that was higher than that of other reported catalysts. The enhanced photocatalytic activities could be attributed to TIPA, a strong electron donor, which can stabilize the charge-transferred state and modify the electrical conductivity of the materials. The results of this work should provide new ideas for the rational design of other MOFs for application in photocatalytic reactions.

Declaration of interest statement

We affirm that all authors have seen and approved the submission of the manuscript. And we promise that: This manuscript is not under consideration for publication elsewhere and that no portion has been published elsewhere in any medium including electronic journals and computer databases of a public nature. The portions of text or wording in the present manuscript have not been duplicated from previous work published by us or by other authors. The authors declare no competing financial interest.

CRedit authorship contribution statement

Guiqin Niu: Data curation, Software, Investigation, Writing – original draft. **Chen Si:** Investigation. **Jiachen Jiao:** Investigation.

Qixia Han: Resources, Writing – review & editing, Supervision, Data curation. **Mengfei Guo:** Investigation. **Mingxue Li:** Writing – review & editing.

Acknowledgements

This work was supported by the Key Scientific Research Project of Henan Higher Education Institutions (grant no.20ZX006), the National Natural Science Foundation of China (No. 21601048, 21671055), Henan University First-class Discipline Cultivation Project (grant no. 2019YLZDJL10).

References

- B. Nanda, A.C. Pradhan, K.M. Parida, Fabrication of mesoporous CuO/ZrO₂-MCM-41 nanocomposites for photocatalytic reduction of Cr(VI), *Chem. Eng. J.* 316 (2017) 1122–1135.
- S. Ghosh, H. Remita, R.N. Basu, Visible-light-induced reduction of Cr(VI) by PDPB-ZnO nanohybrids and its photo-electrochemical response, *Appl. Catal., B* 239 (2018) 362–372.
- J.C. He, J. Li, W. Du, Q.X. Han, Z.L. Wang, M.X. Li, A mesoporous metal-organic framework: potential advances in selective dye adsorption, *J. Alloys Compd.* 750 (2018) 360–367.
- P.H. Shao, D.H. Liang, L.M. Yang, H. Shi, Z.S. Xiong, L. Ding, X.C. Yin, K. Zhang, X.B. Luo, Evaluating the adsorptivity of organo-functionalized silica nanoparticles towards heavy metals: quantitative comparison and mechanistic insight, *J. Hazard Mater.* 387 (2020) 121676.
- P.H. Shao, L. Ding, J.F. Luo, Y. Luo, D. You, Q.G. Zhang, X.B. Luo, Lattice-defect-enhanced adsorption of arsenic on zirconia nanospheres: a combined experimental and theoretical study, *ACS Appl. Mater. Interfaces* 11 (2019) 29736–29745.
- X.C. Yin, P.H. Shao, L. Ding, Y. Xi, K. Zhang, L.M. Yang, H. Shi, X.B. Luo, Protonation of rhodanine polymers for enhancing the capture and recovery of Ag⁺ from highly acidic wastewater, *Environ. Sci. Nano.* 6 (2019) 3307–3315.
- J.T. Sun, Z.P. Zhang, J. Ji, M. Dou, F. Wang, Removal of Cr⁶⁺ from wastewater via adsorption with high-specific-surface-area nitrogen-doped hierarchical porous carbon derived from silkworm cocoon, *Appl. Surf. Sci.* 405 (2017) 372–379.
- Y.X. Wang, H.X. Zhao, X.X. Li, R.H. Wang, A durable luminescent ionic polymer for rapid detection and efficient removal of toxic Cr₂O₇²⁻, *J. Mater. Chem. A* 4 (2016) 12554–12560.
- N.N. Zhang, G.S. Li, S. Wang, X.L. Xu, L.P. Li, TaCxOy: a photocatalytic promoter on g-C₃N₄ for visible-light Cr⁶⁺ reduction, *Catal. Commun.* 119 (2019) 129–133.
- C.L. Chen, K.R. Zhu, K. Chen, A. Alsaedi, T. Hayat, Synthesis of Ag nanoparticles decoration on magnetic carbonized polydopamine nanospheres for effective catalytic reduction of Cr(VI), *J. Colloid Interface Sci.* 526 (2018) 1–8.
- J. Dong, H. Xu, S.L. Hou, Z.L. Wu, B. Zhao, Metal-organic frameworks with Tb₄ clusters as nodes: luminescent detection of chromium(VI) and chemical fixation of CO₂, *Inorg. Chem.* 56 (2017) 6244–6250.
- P.C. Bandara, E.T. Nadres, D.F. Rodrigues, Use of response surface methodology to develop and optimize the composition of a chitosan- polyethyleneimine-graphene oxide nanocomposite membrane coating to more effectively remove Cr(VI) and Cu(II) from water, *ACS Appl. Mater. Interfaces* 11 (2019) 17784–17795.
- Q.Q. Meng, Y.S. Zhou, G. Chen, Y.D. Hu, C.D. Lv, L.S. Qiang, W.N. Xing, Integrating both homojunction and heterojunction in QDs self-decorated Bi₂MoO₆/BCN composites to achieve an efficient photocatalyst for Cr(VI) reduction, *Chem. Eng. J.* 334 (2018) 334–343.
- X.Q. Qiao, Z.W. Zhang, Q.H. Li, D.F. Hou, Q.C. Zhang, J. Zhang, D.S. Li, P.Y. Feng, X.H. Bu, In situ synthesis of n-n Bi₂MoO₆ & Bi₂S₃ heterojunctions for highly efficient photocatalytic removal of Cr(VI), *J. Mater. Chem. A* 6 (2018) 22580–22589.
- X.L. He, Y.P. Liu, K.N. Gong, Z.G. Han, X.L. Zhai, Copper-organic cationic ring with an inserted arsenic-vanadium polyanionic cluster for efficient catalytic Cr^{VI} reduction using formic acid, *Inorg. Chem.* 54 (2015) 1215–1217.
- G. Li, Y. Wu, M. Zhang, B. Chu, W. Huang, M. Fan, L. Dong, B. Li, Enhanced removal of toxic Cr(VI) in wastewater by synthetic TiO₂/g-C₃N₄ microspheres/rGO photocatalyst under irradiation of visible light, *Ind. Eng. Chem. Res.* 58 (2019) 8979–8989.
- H. Zhang, J. Yang, Y.Y. Liu, S.Y. Song, X.L. Liu, J.F. Ma, Visible light photodegradation of organic dyes, reduction of Cr^{VI} and catalytic oxidative desulfurization by a class of polyoxometalate-based inorganic-organic hybrid compounds, *Dyes Pigments* 133 (2016) 189–200.
- B. Vellaichamy, P. Periakaruppan, B. Nagulan, Reduction of Cr⁶⁺ from wastewater using a novel in situ-synthesized PANI/MnO₂/TiO₂ nanocomposite: renewable, selective, stable, and synergistic catalysis, *ACS Sustain. Chem. Eng.* 5 (2017) 9313–9324.
- W.M. Hao, X.Q. Li, L.X. Qin, S. Han, S.Z. Kang, Facile preparation of Ti³⁺ self-doped TiO₂ nanoparticles and their dramatic visible photocatalytic activity

- for the fast treatment of highly concentrated Cr(VI) effluent, *Catal. Sci. Technol.* 9 (2019) 2523–2531.
- [20] G. Yang, Y.J. Liang, K. Li, J. Yang, R. Xu, X.J. Xie, Construction of a Ce³⁺ doped CeO₂/Bi₂MoO₆ heterojunction with a mutual component activation system for highly enhancing the visible-light photocatalytic activity for removal of TC or Cr(VI), *Inorg. Chem. Front.* 6 (2019) 1507–1517.
- [21] Y.H. Zou, J. Liang, C. He, Y.B. Huang, R. Cao, A mesoporous cationic metal-organic framework with a high density of positive charge for enhanced removal of dichromate from water, *Dalton Trans.* 48 (2019) 6680–6684.
- [22] S. Karmakar, D. Roy, C. Janiak, S. De, Insights into multi-component adsorption of reactive dyes on MIL-101-Cr metal organic framework: experimental and modeling approach, *Separ. Purif. Technol.* 215 (2019) 259–275.
- [23] J.M. Li, R. Li, X. Li, Construction of metal-organic frameworks (MOFs) and highly luminescent Eu(III)-MOF for the detection of inorganic ions and antibiotics in aqueous medium, *CrystEngComm* 20 (2018) 4962–4972.
- [24] C.C. Wang, X.H. Yi, P. Wang, Powerful combination of MOFs and C₃N₄ for enhanced photocatalytic performance, *Appl. Catal., B* 247 (2019) 24–48.
- [25] J.C. He, Q.X. Han, J. Li, Z.L. Shi, X.Z. Shi, J.Y. Niu, Ternary supramolecular system for photocatalytic oxidation with air by consecutive photo-induced electron transfer processes, *J. Catal.* 376 (2019) 161–167.
- [26] Y. Fang, Y. Ma, M. Zheng, P. Yang, A.M. Asiri, X. Wang, Metal-organic frameworks for solar energy conversion by photoredox catalysis, *Coord. Chem. Rev.* 373 (2018) 83–115.
- [27] J.D. Xiao, H.L. Jiang, Metal-organic frameworks for photocatalysis and photothermal catalysis, *Acc. Chem. Res.* 52 (2019) 356–366.
- [28] Y. Shang, Y. Wen, S. Li, S. Du, X. He, L. Cai, Y. Li, L. Yang, H. Gao, Y. Song, A triphenylamine-containing donor-acceptor molecule for stable, reversible, ultrahigh density data storage, *J. Am. Chem. Soc.* 129 (2007) 11674–11675.
- [29] R. Rathore, C.L. Burns, I.A. Guzei, Synthesis and isolation of polytrityl cations by utilizing hexaphenylbenzene and tetraphenylmethane scaffolds, *J. Org. Chem.* 69 (2004) 1524–1530.
- [30] Y.J. Xiao, Y. Qi, X.L. Wang, X.Y. Wang, F.X. Zhang, C. Li, Visible-light-responsive 2D cadmium organic framework single crystals with dual functions of water reduction and oxidation, *Adv. Mater.* 30 (2018) 1803401.
- [31] T.Y. Zeng, D.J. Shi, Q.R. Cheng, G.Y. Liao, H. Zhou, Z.Q. Pan, Construction of novel phosphonate-based MOF/P-TiO₂ heterojunction photocatalysts: enhanced photocatalytic performance and mechanistic insight, *Environ. Sci. Nano.* (2020).
- [32] F. Rouhani, R.M. Fatemeh, A. Morsali, Highly electroconductive metal-organic framework: tunable by metal ion sorption quantity, *J. Am. Chem. Soc.* 141 (2019) 11173–11182.
- [33] H.R. Fu, Y. Kang, J. Zhang, Highly selective sorption of small hydrocarbons and photocatalytic properties of three metal-organic frameworks based on tris(4-(1H-imidazol-1-yl)phenyl)amine ligand, *Inorg. Chem.* 53 (2014) 4209–4214.
- [34] H.R. Fu, Y. Zhao, Z. Zhou, X.G. Yang, L.F. Ma, Neutral ligand TIPA-based two 2D metal-organic frameworks: ultrahigh selectivity of C₂H₂/CH₄ and efficient sensing and sorption of Cr(VI), *Dalton Trans.* 47 (2018) 3725–3732.
- [35] X.Q. Yao, D.P. Cao, J.S. Hu, Y.Z. Li, Z.J. Guo, H.G. Zheng, Chiral and porous coordination polymers based on an N-centered triangular rigid ligand, *Cryst. Growth Des.* 11 (2011) 231–239.
- [36] Y. Shen, C.C. Fan, Y.Z. Wei, J. Du, H.B. Zhu, Y. Zhao, Construction of non-interpenetrating and interpenetrating (4-Fold and 8-Fold) 3-D Cd(II) networks with tris(1,2,4-triazol-4-yl)phenyl)amine modulated by aromatic dicarboxylate coligands, *Cryst. Growth Des.* 16 (2016) 5859–5868.
- [37] A.L. Spek, Single-crystal structure validation with the program PLATON, *J. Appl. Crystallogr.* 36 (2003) 7–13.
- [38] J. Li, G.X. Liu, Three cadmium(II) coordination polymers constructed from polycarboxylate and tri(imidazole) ligands: syntheses, crystal structures and luminescent properties, *Polyhedron* 157 (2019) 284–291.
- [39] H. Wu, C.J. Shi, Y.Q. Zhao, Y.T. Jiang, Y.H. Tao, Three coordination polymers based on different carboxylates, metals and a tri(4-imidazolylphenyl)amine ligand, *J. Mol. Struct.* 1086 (2015) 276–281.
- [40] M.X. Li, Z.X. Miao, M. Shao, S.W. Liang, S.R. Zhu, Metal-organic frameworks constructed from 2,4,6-Tris(4-pyridyl)-1,3,5-triazine, *Inorg. Chem.* 47 (2008) 4481–4489.
- [41] C.W. Chang, H.J. Yen, K.Y. Huang, et al., Novel organosoluble aromatic polyimides bearing pendant methoxy-substituted triphenylamine moieties: synthesis, electrochromic, and gas separation properties, *J. Polym. Sci., Part A: Polym. Chem.* 46 (224) (2008) 7937–7949.
- [42] Y.L. Guo, D. Wang, X.Y. Liu, X.D. Wang, W.S. Liu, W.W. Qin, Synthesis and characterization of the nickel@carbon dots hybrid material and its application in the reduction of Cr(VI), *New J. Chem.* 38 (2014) 5861–5867.
- [43] S. Thirumaran, K. Ramalingam, G. Bocelli, L. Righi, XPS, single crystal X-ray diffraction and cyclic voltammetric studies on 1,10-phenanthroline and 2,2'-bipyridine adducts of bis(piperidinecarbodithioato-S,S')cadmium(II) with CdS4N2 environment - a stereochemical and electronic distribution investigation, *Polyhedron* 28 (2009) 263–268.
- [44] H. Wu, H.Y. Liu, Y.Y. Liu, J. Yang, B. Liu, J.F. Ma, An unprecedented 2D-3D metal-organic polyrotaxane framework constructed from cadmium and a flexible star-like ligand, *Chem. Commun.* 47 (2011) 1818–1820.
- [45] Y.Y. Sun, X.J. Chen, F.Y. Wang, R.D. Ma, X.M. Guo, S.W. Sun, H.D. Guo, E.V. Alexandrov, Variation of topologies and entanglements in metal-organic frameworks with mixed tris[4-(1H-imidazol-1-yl)phenyl]phosphine oxide and dicarboxylate ligands, *Dalton Trans.* 48 (2019) 5450–5458.
- [46] H. Wu, H.Y. Liu, J. Yang, B. Liu, J.F. Ma, Y.Y. Liu, Y.Y. Liu, Series of coordination polymers based on different carboxylates and a tri(4-imidazolylphenyl)amine ligand: entangled structures and photoluminescence, *Cryst. Growth Des.* 11 (2011) 2317–2324.
- [47] S.G. Wang, S.Z. Xing, Z.L. Shi, J.C. He, Q.X. Han, M.X. Li, Electrostatic polypyridine-ruthenium(II) decatungstate dyads: structures, characterizations and photodegradation of dye, *RSC Adv.* 7 (2017) 18024–18031.
- [48] H. Wu, H. Chen, M. Fu, R. Li, P. Ma, J. Wang, J. Niu, A PHBA-functionalized organic-inorganic hybrid polyoxometalate as a luminescent probe for selectively sensing chromium and calcium in aqueous solution, *Dyes Pigments* 171 (2019) 107696.
- [49] J.C. He, J. Li, Q.X. Han, C. Si, G.Q. Niu, M.X. Li, J.P. Wang, J.Y. Niu, Photoactive metal-organic framework for the reduction of aryl halides by the synergistic effect of consecutive photo-induced electron-transfer and hydrogen-atom transfer processes, *ACS Appl. Mater. Interfaces* 12 (2020) 2199–2206.
- [50] X.K. Wang, J. Liu, L. Zhang, L.Z. Dong, S.L. Li, Y.H. Kan, D.S. Li, Y.Q. Lan, Monometallic catalytic models hosted in stable metal-organic frameworks for tunable CO₂ photoreduction, *ACS Catal.* 9 (2019) 1726–1732.
- [51] X.S. Wang, C.H. Chen, F. Ichihara, M. Oshikiri, J. Liang, L. Lia, Y.X. Li, H. Song, S.Y. Wang, T. Zhang, Y.B. Huang, R. Cao, J.H. Ye, Integration of adsorption and photosensitivity capabilities into a cationic multivariate metal-organic framework for enhanced visible-light photoreduction reaction, *Appl. Catal., B* 253 (2019) 323–330.
- [52] C. Zhao, Z.H. Wang, X. Li, X.H. Yi, H.Y. Chu, X. Chen, C.C. Wang, Facile fabrication of BUC-21/Bi₂O₃Br₁₀ composites for enhanced photocatalytic Cr(VI) reduction under white light, *Chem. Eng. J.* (2019) 123431.
- [53] Y.C. Zhou, X.Y. Xu, P. Wang, H.F. Fu, C. Zhao, C.C. Wang, Facile fabrication and enhanced photocatalytic performance of visible light responsive UiO-66-NH₂/Ag₂CO₃ composite, *Chin. J. Catal.* 40 (2019) 1912–1923.
- [54] X.H. Yi, S.Q. Ma, X.D. Du, C. Zhao, H.F. Fu, P. Wang, C.C. Wang, The facile fabrication of 2D/3D Z-scheme g-C₃N₄/UiO-66 heterojunction with enhanced photocatalytic Cr(VI) reduction performance under white light, *Chem. Eng. J.* 375 (2019) 121944.
- [55] M. Ghalei, J. Vandeborre, G. Blain, F. Haddad, M. Mostafavi, M. Fattah, Oxidation and/or reduction of manganese species by γ -ray and He⁺ particle irradiation in highly concentrated carbonate media, *Radiat. Phys. Chem.* 119 (2016) 142–150.
- [56] Z.Q. Xia, C. He, X.G. Wang, C.Y. Duan, Modifying electron transfer between photoredox and organocatalytic units via framework interpenetration for β -carbonyl functionalization, *Nat. Commun.* 8 (2017) 361.
- [57] D.D. Chen, X.H. Yi, C. Zhao, H.F. Fu, P. Wang, C.C. Wang, Polyaniiline modified MIL-100(Fe) for enhanced photocatalytic Cr(VI) reduction and tetracycline degradation under white light, *Chemosphere* 245 (2020) 125659.